BMC Biology

RESEARCH

Open Access

Transcriptomic signatures of oxytosis/ferroptosis are enriched in Alzheimer's disease

Antonio Currais[1*], Kayla Sanchez[2], David Soriano-Castell[1], Nawab John Dar[1], K. Garrett Evensen[3], Salvador Soriano[2] and Pamela Maher[1*]

Abstract

Background Oxytosis/ferroptosis is a form of non-apoptotic regulated cell death characterized by specific changes in the redox balance that lead to lethal lipid peroxidation. It has been hypothesized recently that aging predisposes the brain to the activation of oxytosis/ferroptosis in Alzheimer's disease (AD), and consequently that inhibition of oxytosis/ferroptosis offers a path to develop a new class of therapeutics for the disease. The goal of the present study was to investigate the occurrence of oxytosis/ferroptosis in the AD brain by examining transcriptomic signatures of oxytosis/ferroptosis in cellular and animal models of AD as well as in human AD brain samples.

Results Since oxytosis/ferroptosis has been poorly defined at the RNA level, the publicly available datasets are limited. To address this limitation, we developed TrioSig, a gene signature generated from transcriptomic data of human microglia, astrocytes, and neurons treated with inducers of oxytosis/ferroptosis. It is shown that the different signatures of oxytosis/ferroptosis are enriched to varying extents in the brains of AD mice and human AD patients. The TrioSig signature was the most frequently found enriched, and bioinformatic analysis of its composition identified genes involved in the integrated stress response (ISR). It was confirmed in nerve cell culture that oxytosis/ferroptosis induces the ISR via phosphorylation of eukaryotic translation initiation factor 2 alpha (eIF2α) and activating transcription factor 4 (ATF4) signaling.

Conclusions Our data support the involvement of oxytosis/ferroptosis in AD. The implications of the ISR for the progression and prevention of AD are discussed.

Keywords Oxytosis/ferroptosis, Alzheimer's disease, Transcriptomics, Integrated stress response (ISR), Activating transcription factor 4 (ATF4)

Background

Oxytosis is a form of non-apoptotic regulated cell death characterized by glutathione (GSH) depletion and dysregulated production of free radicals from mitochondria that results in lethal lipid peroxidation [1–4]. This pathway was later named ferroptosis when it was redescribed as an iron-dependent, non-apoptotic form of cell death [5], but because the key mechanistic steps are similar, the name oxytosis/ferroptosis has been proposed [3, 4]. Oxytosis/ferroptosis can be triggered by inhibiting cystine uptake via system xc-, which subsequently depletes intracellular GSH, leading to inhibition of the GSH-dependent enzyme GSH peroxidase 4 (GPX4), activation of

*Correspondence:
Antonio Currais
acurrais@salk.edu
Pamela Maher
pmaher@salk.edu
[1] Cellular Neurobiology Laboratory, The Salk Institute for Biological Studies, 10010 N. Torrey Pines Rd, La Jolla, CA 92037, USA
[2] Department of Pathology and Human Anatomy, School of Medicine, Loma Linda University, Loma Linda, CA, USA
[3] The Razavi Newman Integrative Genomics and Bioinformatics Core, The Salk Institute for Biological Studies, 10010 N. Torrey Pines Rd, La Jolla, CA 92037, USA

lipoxygenases (LOXs). and impaired mitochondrial bioenergetics [1–4, 6]. Reactive oxygen species (ROS) and lipid peroxides are generated, which potentiate intracellular calcium (Ca^{2+}) influx through store-operated Ca^{2+} channels, leading to cell death [4, 7].

Importantly, most of these events are observed in the central nervous system (CNS) with aging and are exacerbated in Alzheimer's disease (AD) [4, 8–12]. The levels of GSH in the human brain and blood decrease with age and are further reduced in AD [13–23]. The loss of GSH is associated with impairments in cognitive function, microglial activation, and endothelial dysfunction [2, 16].

In addition, postmortem brain samples from subjects with mild cognitive impairment (MCI) already show increased levels of lipid peroxidation, and by-products of lipid peroxidation in plasma, urine, and cerebrospinal fluid (CSF) are elevated throughout the progression of the disease [8, 24–27], with several LOXs implicated in AD [28–31].

A decline in cerebral energy metabolism, similar to what happens during oxytosis/ferroptosis [4, 32], is observed with aging and is one of the earliest events in AD [33–36]. Moreover, aging is associated with imbalances in iron metabolism and disruption in metal homeostasis is an important feature in AD [8, 37–39]. Selective accumulation of iron has been detected in neurofibrillary tangles [40] as well as specific brain regions [41] and is associated with hippocampal damage [42] and the rate of cognitive decline in AD patients [43].

Finally, it has been shown that intracellular accumulation of amyloid beta (Aβ) can induce oxytosis/ferroptosis associated with the expression of pro-inflammatory mediators and metabolic alterations characterized by deficits in glucose metabolism and mitochondrial bioenergetics [44], and that genetic ablation of *GPX4* specifically in neurons causes neurodegeneration in mice associated with neuroinflammation [45, 46].

Given all of this evidence, we have hypothesized recently that activation of oxytosis/ferroptosis in the brain with aging contributes to AD [4], and consequently that inhibition of oxytosis/ferroptosis offers a path to develop a new class of therapeutics for the disease [47, 48]. The goal of the present study was to investigate the occurrence of oxytosis/ferroptosis in the AD brain by examining transcriptomic signatures of oxytosis/ferroptosis in multiple cellular and animal models of AD as well as in human AD brain samples. Collectively, our data show that three different signatures of oxytosis/ferroptosis are enriched to varying extents in the brains of AD mice and human AD patients, with this enrichment being observed in multiple cell types. Moreover, we found that the signature with the best enrichment—TrioSig—is enriched in genes involved in the integrated stress response (ISR). We confirmed that exposure of nerve cells in culture to inducers of oxytosis/ferroptosis triggers the ISR via phosphorylation of eukaryotic translation initiation factor 2 alpha (eIF2α) and activating transcription factor 4 (ATF4) signaling. The implications of ISR activation for oxytosis/ferroptosis and AD are discussed.

Results

Briefly, the following experimental approach was carried out. Since oxytosis/ferroptosis has been poorly defined at the RNA level, the publicly available datasets are limited. Therefore, we started our study by developing a gene signature generated from transcriptomic data of human brain cells treated with inducers of oxytosis/ferroptosis. We first validated this signature and the others publicly available in cell culture systems where oxytosis/ferroptosis is activated. We then tested the signatures in multiple animal models of AD and in human AD brain samples, examining transcriptomic data from different brain regions as well as specific brain cell types. Finally, we analyzed bioinformatically the various signatures and mechanistically studied key underlying molecular pathways in cell culture.

Selection of gene signatures of oxytosis/ferroptosis

To determine whether genes associated with oxytosis/ferroptosis are enriched in biological samples, specific gene sets are required. In this study, we tested three different gene sets relevant to oxytosis/ferroptosis: the Kyoto Encyclopedia of Genes and Genomes (KEGG) Ferroptosis pathway, the Ferroptosis Database (FerrDb) [49, 50], and a set that we defined based on transcriptomic data from human iPSC-derived brain cells grown in a tri-culture system (neurons, astrocytes, and microglia) and exposed to inducers of oxytosis/ferroptosis [51].

The KEGG gene set includes 41 and 40 genes associated with ferroptosis in humans and mice, respectively (Supplementary Table 1). These are the genes commonly tested by most of the enrichment analysis software that use publicly available databases. The FerrDb was recently introduced [49], with an updated version [50], as a manually curated database that includes 539 regulators and markers of ferroptosis (Supplementary Table 1). Since neither the KEGG nor FerrDb signatures were assembled from direct transcriptomics of cells undergoing oxytosis/ferroptosis, we developed a new gene signature of oxytosis/ferroptosis by using RNAseq data obtained by the Hammond lab from human iPSC-derived microglia, astrocytes, and neurons grown in tri-culture and exposed to RSL3 (an inhibitor of GPX4) as well as iron to induce oxytosis/ferroptosis [51]. The differentially expressed (DE) genes in each of these cell types were overlapped to identify changes that were shared. We

undertook this approach because our ultimate goal was to analyze published RNAseq data from brain regions of AD patients, which contain heterogeneous cell type populations. Having a signature of genes associated with oxytosis/ferroptosis in different cell types would thus increase the chances of detecting a signal when analyzing whole brain tissues. The initial overlap identified 545 DE genes between untreated tri-cultures and tri-cultures treated with RSL3/iron (Supplementary Table 2). To narrow down this number and potentially increase the sensitivity of the signature, we overlapped the DE genes by direction of expression. This approach identified 109 shared DE genes that were upregulated and 200 that were downregulated with oxytosis/ferroptosis induction in triculture of microglia, astrocytes, and neurons. A total of 309 DE genes (290 homologue mouse genes) were used as the new signature—TrioSig (Supplementary Table 1). Overlap of the FerrDb, TrioSig, and Ferroptosis signatures showed that they are quite distinct in composition (Fig. 1A).

We also investigated the enrichment of other forms of cell death that are listed in the KEGG database, specifically apoptosis and necroptosis (Supplementary Table 1). In addition, we included autophagy because it can be a mechanism of cell death and because there are reports indicating an interaction between autophagy and oxytosis/ferroptosis [52]. These gene sets shared a low number of genes with the FerrDb, TrioSig, and Ferroptosis gene sets, with the Ferroptosis gene set having the highest relative overlap and the TrioSig gene set having the lowest relative overlap (Supplementary Fig. 1).

We next aimed to understand how these signatures were related to the transcriptomic identity of key brain cell types (astrocytes, endothelial cells, microglia, neurons, and oligodendrocytes). We used three measures of human and mouse brain cell type-relative expression (top 1000 genes), including specificity, enrichment, and absolute expression [53]. For absolute expression, the cell type-specific genes are selected based on their relative expression in a particular cell type irrespective of that in other cell types. In cell type enrichment, the genes are selected by measuring the expression of each gene relative to the expression of that gene in all other cell types. With this measure, a gene could have relatively high expression in two cell types and be relatively enriched in each of them compared to all other cell types. For specificity, the genes are defined by the expression of each gene relative to the highest expression of that gene in all other cell types. This requires that the expression of the gene is only high in one cell type [53]. Analysis of the FerrDb, TrioSig, and Ferroptosis signatures using absolute expression showed that the signatures were significantly enriched across cell types in both the human and mouse datasets (Fig. 1B). Enrichment of apoptosis and necroptosis was consistently observed almost exclusively in microglia. When analyzing the signatures using the enrichment measure, only the TrioSig was consistent between human and mouse and observed in microglia. This was confirmed with the specificity measure. These data indicate that the FerrDb, TrioSig, and Ferroptosis signatures are enriched in genes with high expression across all cell types under physiological conditions, and that this expression is highest in microglia.

Validation of gene signatures in cell culture models of oxytosis/ferroptosis

To determine whether the Ferroptosis, FerrDb, and TrioSig signatures could be used to identify the induction of oxytosis/ferroptosis, we first tested their enrichment with transcriptomic data from cell culture models where oxytosis/ferroptosis was experimentally activated. These models included not only the original human iPSC-derived microglia, astrocytes, and neurons used to generate the TrioSig signature but also HT22 mouse hippocampal nerve cells exposed to glutamate [2] and MC65 human neuroblastoma cells induced to aggregate Aβ intracellularly, which causes oxytosis/ferroptosis [44] (Supplementary Tables 2 and 3). We analyzed all DE genes together as well as separated by direction of expression for each of the cell models.

As expected, the iPSC-derived microglia, astrocytes, and neurons were enriched for the TrioSig gene set

(See figure on next page.)

Fig. 1 Selection of gene signatures of oxytosis/ferroptosis and validation in cell culture models of oxytosis/ferroptosis. **A** Overlap of the FerrDb, TrioSig, and Ferroptosis signatures. **B** Enrichment of the FerrDb, TrioSig, Ferroptosis, Apoptosis, Necroptosis, and Autophagy signatures in three transcriptomic measures of human and mouse brain cell type-relative expression, including absolute expression (the cell type-specific genes are selected based on their relative expression in a particular cell type irrespective of that in other cell types), enrichment (the genes are selected by measuring the expression of each gene relative to the expression of that gene in all other cell types), and specificity (the genes are defined by the expression of each gene relative to the highest expression of that gene in all other cell types). **C** Enrichment of the FerrDb, TrioSig, and Ferroptosis signatures in transcriptomic data (DE genes between control and toxicity) from cell culture models where oxytosis/ferroptosis was activated: the original human microglia, astrocytes, and neurons used to generate the TrioSig signature, HT22 mouse hippocampal nerve cells exposed to glutamate, and MC65 human neuroblastoma cells induced to aggregate Aβ intracellularly. Enrichment of Apoptosis, Necroptosis, and Autophagy was also assessed. All DE genes together as well as separated by direction of expression (Down and Up) were analyzed

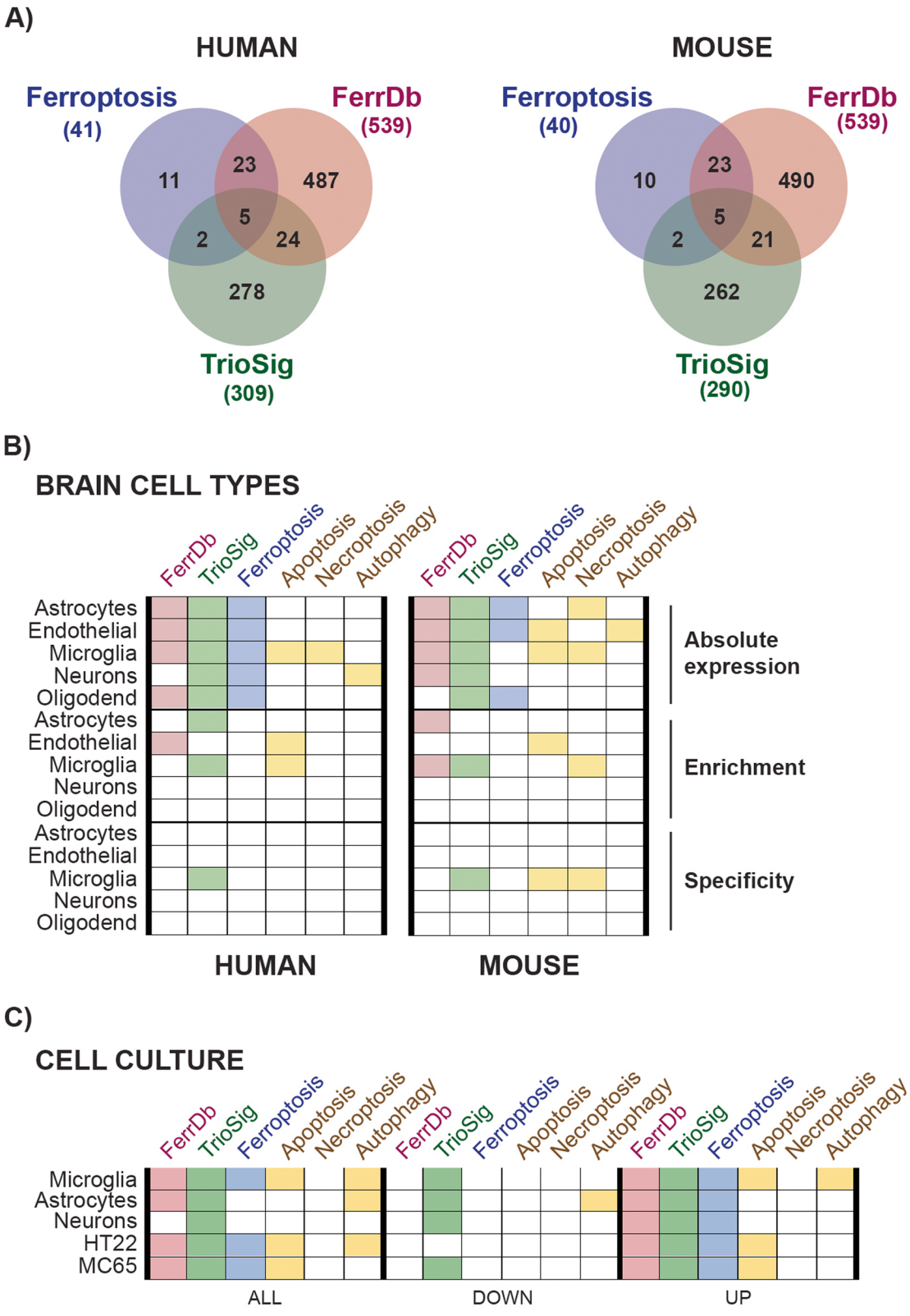

Fig. 1 (See legend on previous page.)

(Fig. 1C). Interestingly, microglia, which were the cell type most responsive to the induction of oxytosis/ferroptosis in the original study [51], were also enriched for the FerrDb and Ferroptosis gene sets. Moreover, all three cell types were enriched for the FerrDb, TrioSig, and Ferroptosis gene sets only in the upregulated DE gene subset, while only in microglia the TrioSig signature was enriched in the downregulated genes. Similar to microglia, the transcriptomes of HT22 cells and MC65 cells undergoing oxytosis/ferroptosis were significantly enriched for the FerrDb, TrioSig, and Ferroptosis gene sets, which were also predominantly detected in the upregulated gene subset. Regarding the other cell death processes, only apoptosis was consistently identified, and this cell death pathway was specifically associated with the upregulated genes (Fig. 1C).

Taken together, these data indicate that all three RNA signatures can be used to detect changes associated with oxytosis/ferroptosis in diverse cell culture models, and that these transcriptomic changes appear to be associated predominantly with upregulated gene expression.

Transcriptomic enrichment of oxytosis/ferroptosis in mouse models and human AD

We next evaluated the oxytosis/ferroptosis gene signatures in brain tissues from multiple mouse models of AD at different ages using the DE genes between diseased mice and age-matched wildtype mice. These included the hAβ-KI (MODEL-AD consortium [54]), APP/PS1 [55], 3xTg-AD (MODEL-AD consortium [54] and [56]), and 5xFAD mouse models (MODEL-AD consortium [54]). Except for the hippocampi of 22-month-old hAβ-KI females and brains of 8-month-old APP/PS1 males, which were primarily enriched for the TrioSig gene set, no significant enrichment was detected in the rest of the hAβ-KI, APP/PS1, and 3xTg-AD data sets that were analyzed (Fig. 2A). On the other hand, the transcriptomic changes in the cortices and hippocampi of both male and female 5xFAD mice were highly enriched for the FerrDb, TrioSig, and Ferroptosis signatures. This was verified in data from two different studies (UCI and JAX), appeared to be age dependent, and, similar to the cell culture results, was particularly noticeable in the upregulated DE gene subset. An enrichment in the Apoptosis and Necroptosis pathways was also observed in the same samples.

Importantly, when analyzing RNAseq data from three major studies with human AD patients (Mayo, ROSMAP, and MSBB) that were harmonized to allow the comparison of DE genes between AD patients and healthy age-matched controls in seven different brain regions (Synapse: syn2580853), the FerrDb and TrioSig signatures were significantly enriched in the temporal cortex (TCX), inferior frontal gyrus (IFG), parahippocampal gyrus (PHG), and superior temporal gyrus (STG) (Fig. 2B). Just as with the AD mice data, this enrichment was predominant in the upregulated genes and was observed together with enrichment in the Apoptosis pathway. Similar observations were made with the male and female data separately. Interestingly, with the exception of the TCX, no enrichment was detected for the Ferroptosis KEGG pathway in any of the human samples. Analysis of the hippocampal AD transcriptome from another study [57] produced similar results, with the FerrDb, TrioSig, and Apoptosis gene sets enriched in AD patients relative to normal controls and predominantly associated with the upregulated gene subset. No consistent enrichment in all genes was found in the cerebellum (CBE), a region thought to be less affected in AD, or in the dorsolateral prefrontal cortex (DLPFC), anterior cingulate cortex (ACC), posterior cingulate cortex (PCC), and frontal pole (FP). However, the TrioSig gene set was enriched in the upregulated genes in the DLPFC and PCC. These findings could reflect pathological alterations taking place in some of these regions that are less related to oxytosis/ferroptosis as well as the time course of disease progression through the brain.

A nominated list of genes that may be good targets for new AD treatments or prevention has been identified using computational analyses of high-dimensional genomic, proteomic, and/or metabolomic data derived from human samples [58]. Interestingly, analysis of these genes also identified a significant enrichment in the FerrDb, TrioSig, and Apoptosis gene sets (Fig. 2C).

Overall, these data show that there is an enrichment in oxytosis/ferroptosis gene signatures in some AD mouse models as well as human AD patients, and that this enrichment is mainly associated with DE genes showing increased expression, similar to what was found with the cell culture data analysis (Fig. 1C).

Single-cell enrichment analysis

The next question was whether the association of transcriptomic signatures of oxytosis/ferroptosis observed in brains of AD mice and AD human patients could be explained by transcriptomic changes in specific cell types. Recently, single-nucleus RNA sequencing (snRNA-seq) has enabled large-scale characterization of transcriptomic profiles of individual cells from brain tissues. We first addressed this question with snRNA-seq data from the cortex of 7-month-old 5xFAD and Wt control mice [59]. We found that the TrioSig gene set was significantly enriched in all cell types where DE genes were detected, including oligodendrocytes, microglia, and neurons, and was mostly associated with

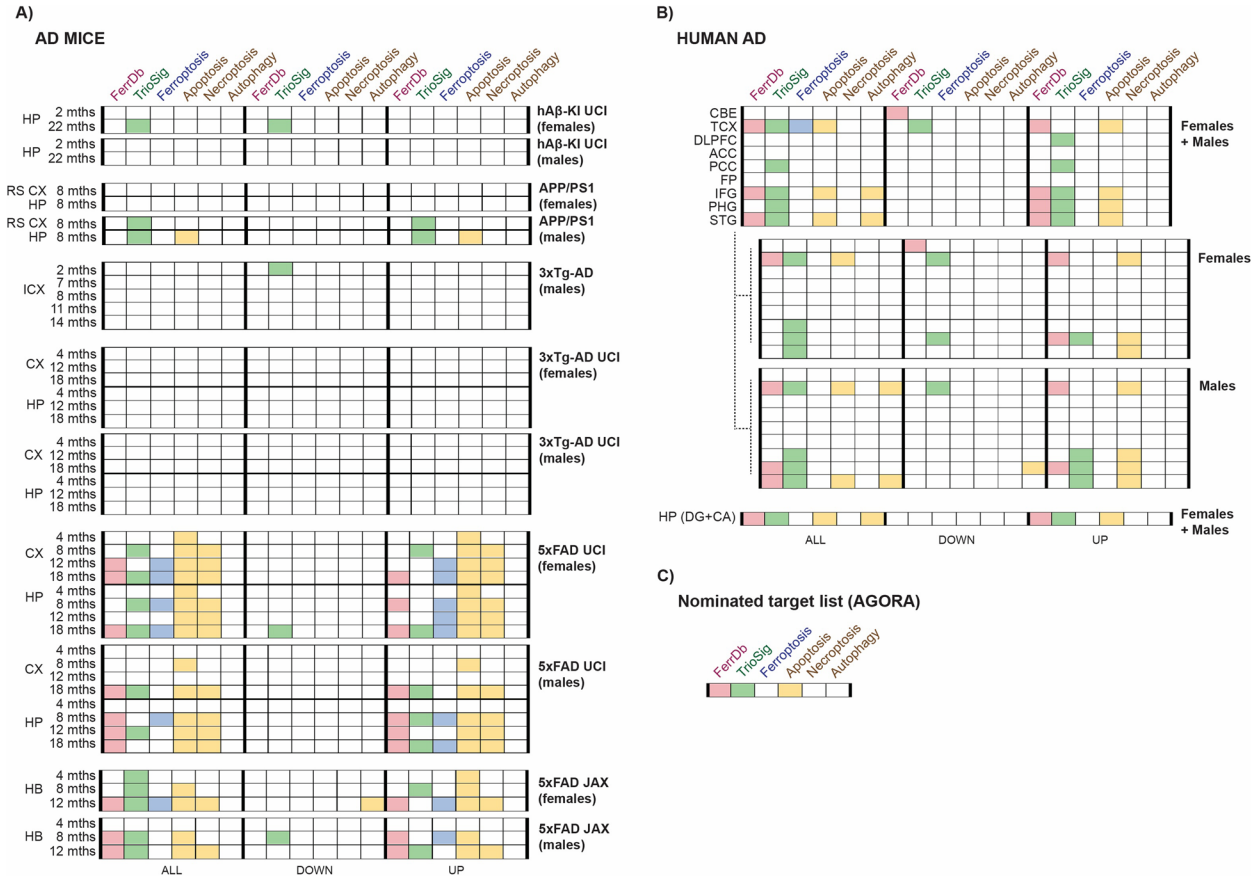

Fig. 2 Transcriptomic enrichment of oxytosis/ferroptosis in mouse models and human AD. **A** Enrichment of the FerrDb, TrioSig, Ferroptosis, Apoptosis, Necroptosis, and Autophagy signatures in transcriptomic data (DE genes between control and disease) of several brain regions from hAβ-KI, APP/PS1, 3xTg-AD, and 5xFAD mouse models of AD. HP, hippocampus; RS CX, retrosplenial cortex; ICX, insular cortex; HB, hemibrain. **B** Enrichment of the FerrDb, TrioSig, Ferroptosis, Apoptosis, Necroptosis, and Autophagy signatures in transcriptomic data (DE genes between control and AD) of several brain regions from human AD patients. CBE, cerebellum; TCX, temporal cortex; DLPFC, dorsolateral prefrontal cortex; ACC, anterior cingulate cortex; PCC, posterior cingulate cortex; FP, frontal pole; IFG, inferior frontal gyrus; PHG, parahippocampal gyrus; STG, superior temporal gyrus; HP, hippocampus; DG, dentate gyrus; CA, cornu ammonis. All DE genes together as well as separated by direction of expression (Down and Up) were analyzed. **C** Enrichment of the FerrDb, TrioSig, Ferroptosis, Apoptosis, Necroptosis, and Autophagy signatures in a nominated list of genes that may be good targets for new AD treatments or prevention (Agora)

the upregulated genes (Fig. 3A). The FerrDb gene set was also enriched in neurons.

We next analyzed snRNA-seq data from the prefrontal cortex (PFC) of human patients with pathologic and cognitive diagnosis of AD versus age-matched healthy controls from the ROSMAP study, published by Mathys et al. [60]. Figure 3B shows an enrichment of the TrioSig gene set across most of the different cell types analyzed from the PFC that generated DE genes, including astrocytes, excitatory and inhibitory neurons, microglia, and OPCs. This enrichment was predominantly seen in the upregulated gene pool. AD in this study was defined based on the modified NIA-Reagan diagnosis of AD which reflects a combination of Braak score and CERAD AD (amyloid plaques and neurofibrillary tangles of microtubule associated protein tau).

In another study, single-cell transcriptomic profiles were obtained from the superior frontal gyrus (SFG) and caudal entorhinal cortex (EC), two brain regions where neurofibrillary inclusions and neuronal loss occur late and early in AD, respectively [61]. This analysis was done on postmortem brains from individuals spanning the progression of AD based on tau neurofibrillary pathology (Braak stages). Analysis of DE genes between healthy controls and AD patients with early stages of tau pathology (Braak 0 vs 2) showed an enrichment of the TrioSig gene set across the different cell types in the SFG and EC in both the down- and

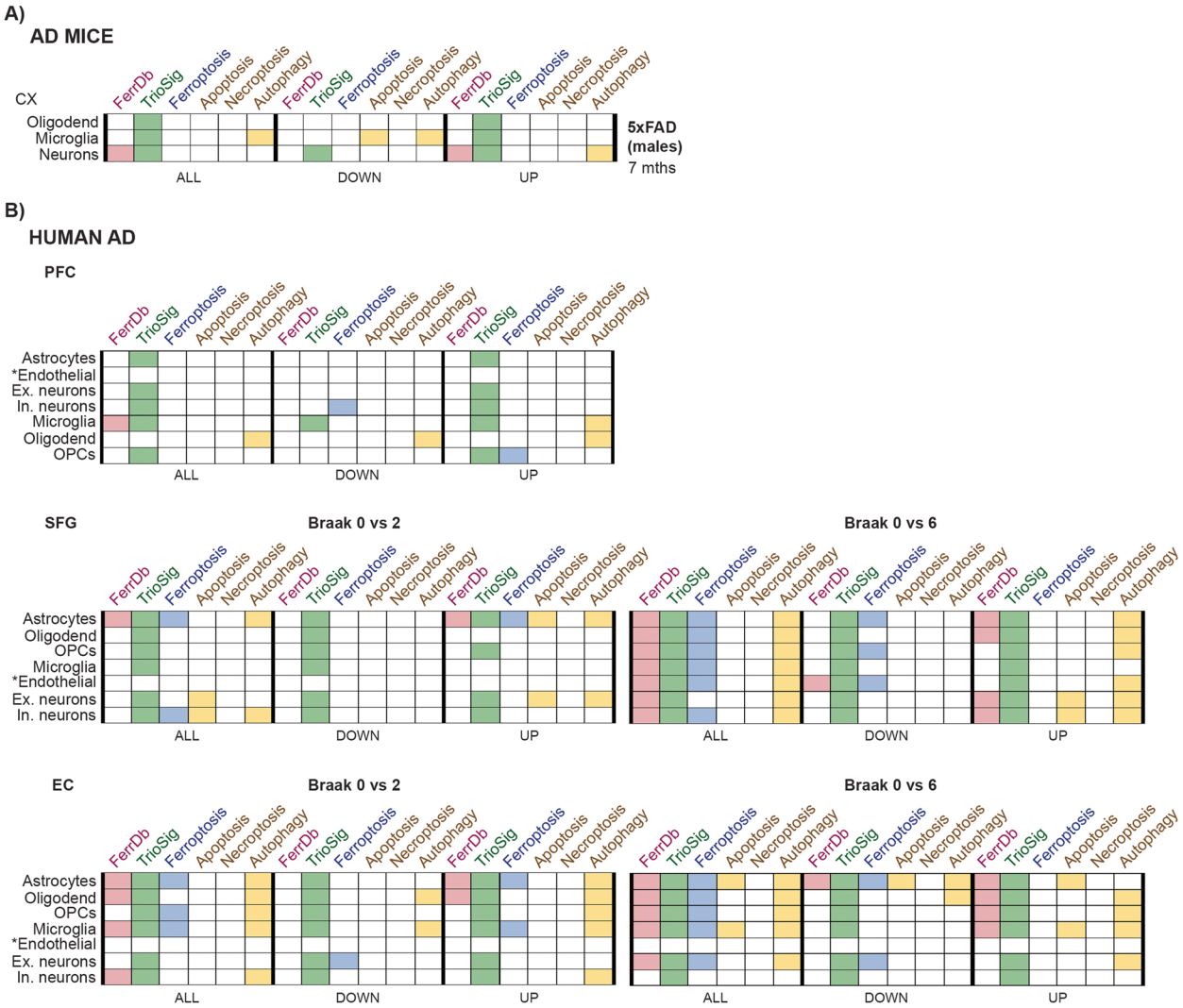

Fig. 3 Single-cell enrichment analysis. **A** Enrichment of the FerrDb, TrioSig, Ferroptosis, Apoptosis, Necroptosis, and Autophagy signatures in single-cell transcriptomic data (DE genes between control and disease) of 5xFAD male mice. CX, cortex. All DE genes together as well as separated by direction of expression (Down and Up) were analyzed. **B** Enrichment of the FerrDb, TrioSig, Ferroptosis, Apoptosis, Necroptosis, and Autophagy signatures in single-cell transcriptomic data (DE genes between control and AD) of several brain regions from human AD patients. PFC, prefrontal cortex; SFG, superior frontal gyrus; EC, caudal entorhinal cortex. All DE genes together as well as separated by direction of expression (Down and Up) were analyzed

upregulated gene pools (Fig. 3B). Interestingly, there was little enrichment for the FerrDb and Ferroptosis gene sets in the SFG but more so in the EC when comparing Braak 0 vs 2. Furthermore, at advanced stages of tau pathology (Braak 0 vs 6), both the SFG and EC were considerably more enriched in the TrioSig, FerrDb, and Ferroptosis signatures across cell types (Fig. 3B). The FerrDb gene set was associated more often with the upregulated gene pool. Enrichment for Autophagy followed a similar trend as the TrioSig gene set, but no pattern was found with the Apoptosis gene set.

Given the observation that the TrioSig gene set was more often observed in the upregulated DE gene pool in cell culture (Fig. 1C), AD mouse models (Fig. 2A), and AD brain regions (Fig. 2B) but not in the individual cell types in the AD brain (Fig. 3B), we re-analyzed all of the data with the TrioSig signature separated into gene sets according to their downregulation and upregulation in the original tri-culture study [51] yielding TrioSig Down and TrioSig Up, respectively. We found that the TrioSig Down gene set was consistently enriched in the DE downregulated gene pool across data sets from the cell

culture studies, mouse models, AD brain regions, and even single-cell types from AD PFC, SFG, and EC (Supplementary Fig. 2). However, the data associated with the upregulated DE genes showed a mixed enrichment in both the TrioSig Down and TrioSig Up signatures.

Altogether, these data suggest that the enrichment of genes associated with the oxytosis/ferroptosis pathway in the brains of AD patients is taking place across different cell types in the brain, and that these changes can vary with the evolution of the disease. Genes associated with the TrioSig signature appear to be activated at earlier stages of the disease, while the expression of genes associated with the FerrDb and Ferroptosis signatures is altered with more advanced pathology. This is consistent with what we found with the cell culture data (Fig. 1C) and the data from the 5xFAD mouse model (Fig. 2A), which is a more aggressive strain then the other AD mouse strains analyzed. In addition, there seems to be an association between the direction of gene expression with pathology and the TrioSig Down and TrioSig Up DE genes which we explored next.

Functional analysis of TrioSig

To understand the pathways underlying the TrioSig signature and the implications of those functions to oxytosis/ferroptosis as well as the AD mouse and human AD brain data, we analyzed the TrioSig bioinformatically. For simplicity, the TrioSig associated with the human genes was used, which includes practically all of the respective mouse homologues. The gene ontology (GO) analysis on biological processes, cellular component, and molecular function consistently identified enriched GO terms related to responses to oxidative stress (red arrows) and ribosomal translation (green arrows) (Fig. 4A).

Pathway analysis with ingenuity pathway analysis (IPA) using the TrioSig gene set including both directions of expression (TrioSig Down + TrioSig Up) determined that the enrichment associated with responses to oxidative stress (nuclear factor erythroid 2-related factor 2 (NFE2L2 or NRF2) is a key transcription factor for multiple antioxidant proteins) was observed in the upregulated gene pool of the TrioSig, while the changes related to ribosomal translation were observed in the downregulated TrioSig genes (Fig. 4B). Parallel analysis of the three signatures TrioSig, FerrDb, and Ferroptosis showed that while all of them were enriched for the antioxidant stress response, only the TrioSig showed enrichment for protein translation (Fig. 4C). Importantly, these observations with TrioSig are indicative of activation of the integrated stress response (ISR). The ISR is an adaptive pathway triggered to restore cellular homeostasis during diverse stress stimuli. It involves the phosphorylation eIF2α, which leads to a decrease in 5′ Cap-dependent protein synthesis and concomitant translation of selected mRNAs that contain a short upstream open reading frame (uORF) in their 5′ untranslated region, namely activating transcription factor 4 (ATF4) [62], which is part of the TrioSig Up. ATF4 cannot only cooperate with but also increase the transcription of NRF2 [63] to control the expression of genes involved in cellular

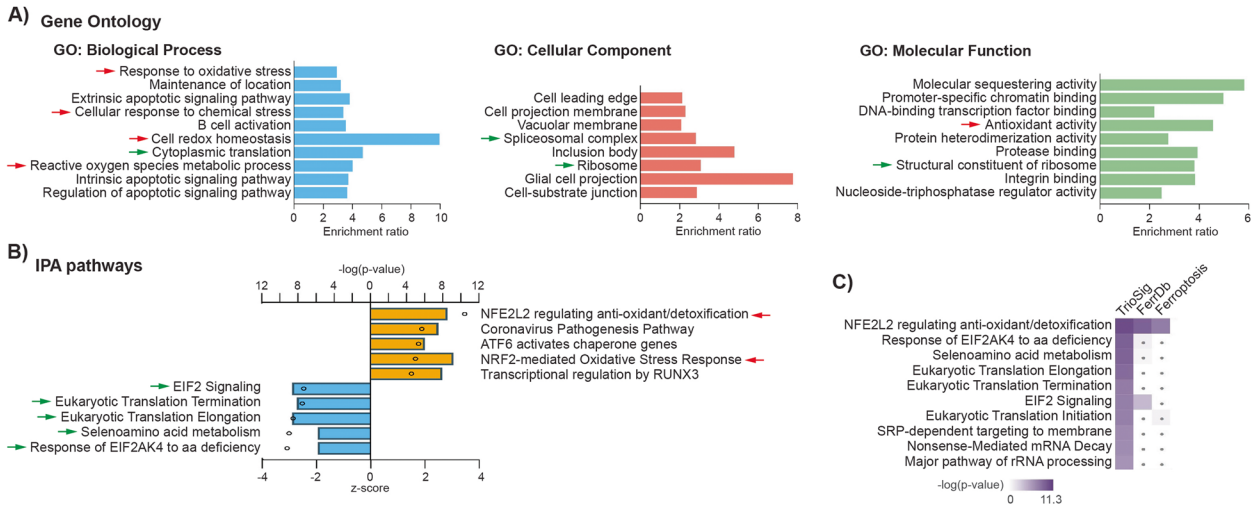

Fig. 4 Bioinformatic analysis of the TrioSig gene set. **A** Gene ontology (GO) analysis of biological processes, cellular component, and molecular function. Red arrows indicate GO terms related to responses to oxidative stress. Green arrows indicate GO terms related to ribosomal translation. **B** Pathway analysis with ingenuity pathway analysis (IPA) using the TrioSig gene set including both directions of expression (TrioSig Down + TrioSig Up). Bar scale is *z*-score. Circle scale is − log(*P* value). **C** IPA analysis of the TrioSig, FerrDb, and Ferroptosis signatures, ordered by the most significant pathways in TrioSig

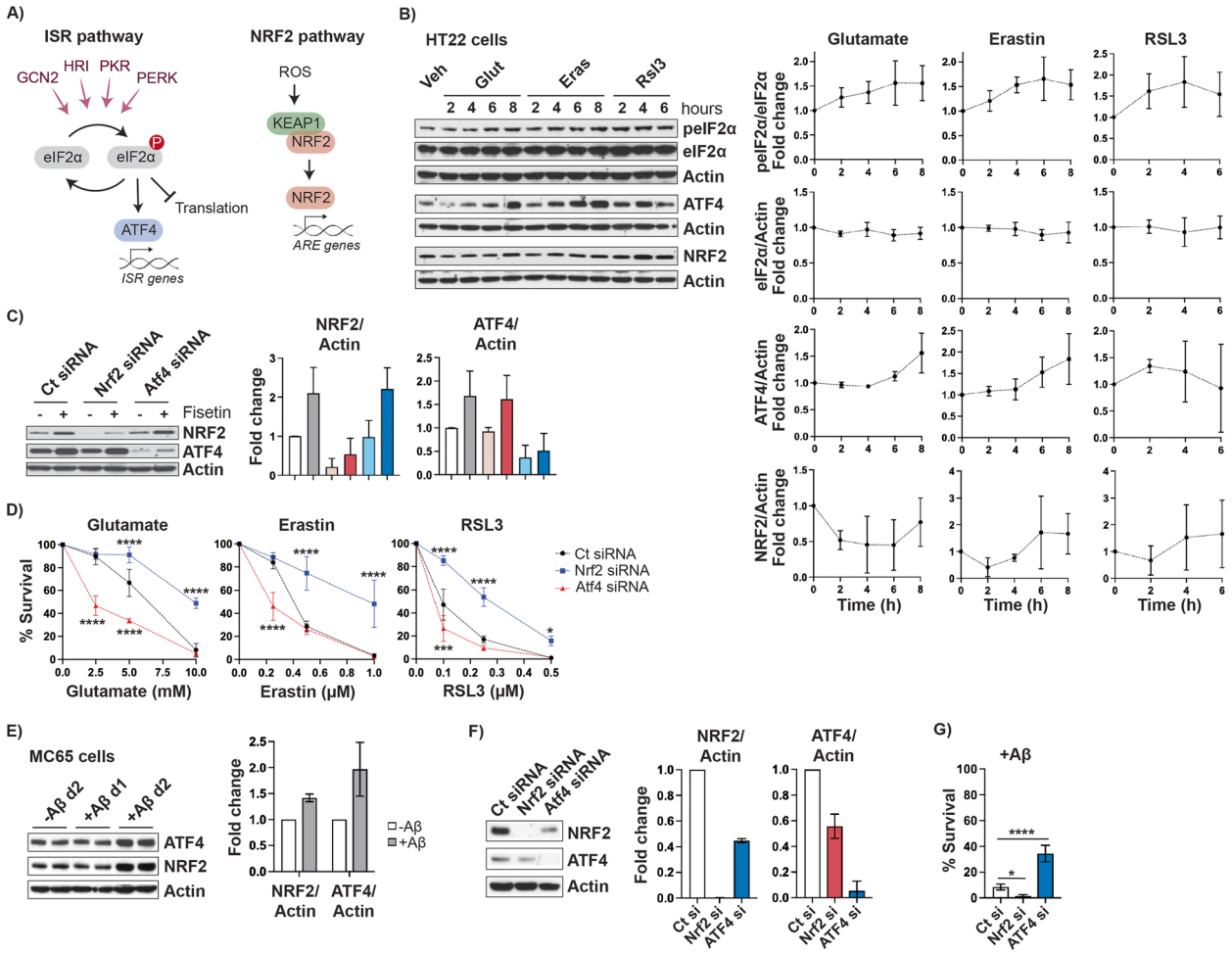

Fig. 5 Mechanistic validation of the TrioSig gene set in cell culture. **A** Diagram of the ISR and NRF2 pathways. **B** Levels of peIF2α, total eIF2α, NRF2, ATF4, and actin after treatment of HT22 cells with 5 mM glutamate, 500 nM erastin, and 250 nM RSL3 at various timepoints were assessed by western blotting and quantified ($n = 3$–4/condition). **C** Levels of NRF2, ATF4, and actin after knockdown with control (Ct), Nrf2, or Atf4 siRNAs ($n = 7$/condition). **D** Survival of HT22 cells exposed to varying concentrations of glutamate, erastin, or RSL3 after knockdown with Ct, Nrf2, or Atf4 siRNAs ($n = 4$/condition). **E** Levels of NRF2, ATF4, and actin in MC65 cells without (− Aβ) and with (+ Aβ) intracellular Aβ aggregation after 1 day (d1) and 2 days (d2), assessed by western blotting and quantified ($n = 3$/condition). **F** Levels of NRF2, ATF4, and actin after knockdown with control (Ct), Nrf2, or Atf4 siRNAs ($n = 3$/condition). **G** Survival of MC65 cells exposed to Aβ toxicity after knockdown with Ct, Nrf2, or Atf4 siRNAs 3 days later ($n = 4$–5/condition). Two-way repeated measures ANOVA and Tukey's multiple comparisons test, $^{*}P < 0.05$, $^{**}P < 0.01$, $^{***}P < 0.001$, $^{****}P < 0.0001$. All data are mean ± SD

adaptation (Fig. 5A). IPA with upstream or downstream regulators of the translation/eIF2 signaling pathway identified repression of translation and activation of ATF4 (Supplementary Fig. 3). IPA of the NRF2 pathway confirmed an upregulation in multiple targets of NRF2 in the TrioSig signature, including the essential genes for GSH metabolism glutamate-cysteine ligase catalytic subunit (GCLC), glutamate-cysteine ligase modifier subunit (GCLM), glutathione-disulfide reductase (GSR) and solute carrier family 7 member 11 (SLC7A11), and the antioxidant enzymes heme oxygenase 1 (HMOX1), peroxiredoxin-1 (PRDX1), sulfiredoxin 1 (SRX1), and thioredoxin reductase 1 (TXRND1) (Supplementary Fig. 4). Interestingly, both the eIF2 and NRF2 pathways predicted upregulation of nuclear protein 1 (NUPR1) as an upstream regulator. NUPR1 is a transcriptional regulator of cellular stress, including oxidative stress that has been shown to repress oxytosis/ferroptosis [64].

To further explore these findings, we examined changes in the molecular signaling of these pathways in HT22 nerve cells exposed to three inducers of oxytosis/ferroptosis: glutamate and erastin (inhibitors of cystine uptake via system X_c^-) and RSL3 (inhibitor of GPX4). Figure 5B shows that glutamate, erastin, and RSL3 induce

robust eIF2α phosphorylation as well as the translocation of ATF4 into the nucleus, indicative of its activation as a transcriptional regulator. Although not as clear due to high variability, the levels of nuclear NRF2 also appear to increase with erastin and RSL3, but not glutamate. Surprisingly, while knockdown of Atf4 enhanced the toxicity by glutamate, erastin, and RSL3, knockdown of Nrf2 slightly protected against these inducers of oxytosis/ferroptosis (Fig. 5C and D). Figure 5C shows the successful knockdowns in combination with fisetin, a flavonoid compound that we previously showed to inhibit oxytosis/ferroptosis while activating both NRF2 and ATF4 [65]. Interestingly, we found that ATF4, but not NRF2, was important for fisetin's ability to protect HT22 cells against glutamate toxicity [65]. Knockdown of either Nrf2 or Atf4 did not alter the expression of the other (Fig. 5C). Because NRF2 regulates protective antioxidant responses that have been reported to inhibit oxytosis/ferroptosis in several cancer cell lines [66, 67], our findings were unexpected. Heme oxygenase-1 (HO1) is a downstream effector of NRF2 that has been shown to potentiate oxytosis/ferroptosis [68, 69]. We confirmed that HO1 expression was elevated in HT22 cells treated with glutamate, erastin, or RSL3, and that knockdown of NRF2 prevented that increase (Supplementary Fig. 5A). Accordingly, inhibiting HO1 with its selective chemical inhibitor zinc protoporphyrin IX (ZnPPIX) or using specific siRNA protected cells against the three inducers of oxytosis/ferroptosis (Supplementary Fig. 5A–C).

We also studied MC65 cells, where intracellular aggregation of Aβ causes oxytosis/ferroptosis [44] associated with transcriptomic enrichment of the TrioSig gene set (Fig. 1C). Similar to HT22 cells, we observed an increase in the expression of both NRF2 and ATF4 2 days after induction of Aβ (Fig. 5E). No changes were identified in eIF2α phosphorylation (not shown), perhaps due to the timing of the signaling. However, unlike in HT22 cells, while knockdown of Atf4 slightly protected against Aβ toxicity, knockdown of Nrf2 enhanced the cell death (Fig. 5G). Knockdown of Nrf2 or Atf4 reduced the expression of the other (Fig. 5F).

These data indicate that the TrioSig is characterized by ISR activation, which is observed during oxytosis/ferroptosis in cell culture.

Discussion

Although some of the key molecular steps of oxytosis/ferroptosis were identified a long time ago [2], only in the past decade has the relevance of this toxicity mechanism to human diseases been brought to light. We have hypothesized recently that oxytosis/ferroptosis is a main contributor to the pathology in AD [4]. The present study supports this hypothesis by showing that different transcriptomic signatures of oxytosis/ferroptosis are enriched to varying extents in the brains of human AD patients (Figs. 2B and 3B).

Several studies have looked at transcriptomic changes in AD brain regions. A meta-analysis performed with data from the Mayo, ROSMAP, and MSBB studies found a significant overlap between gene expression in brains from AD transgenic mice and some AD-associated co-expression modules from human brains [70]. Interestingly, the most robust overlaps were detected among modules enriched for microglial and neuronal genes, which were also enriched in brains from aged mice as well as brains from other disease mouse models. This was associated with the expression of genes implicated in immune biology and inflammation. In fact, results from RNA sequencing of human postmortem brain tissues have pointed out consistently the relevance of microglial and neuroinflammatory processes for the pathology [71–74] and are supported by other molecular findings demonstrating the activation of inflammatory mechanisms in the AD brain [75, 76]. None of the transcriptomic studies identified enrichment of the oxytosis/ferroptosis pathway. This is likely because the gene signature for this pathway that is publicly available is the Ferroptosis pathway in the KEGG database. The majority of our analyses with the AD human brain tissue data did not find this pathway enriched either. The fact that, unlike Ferroptosis, the FerrDb and TrioSig signatures were found enriched in specific tissues indicates that most studies could be missing a potential involvement of oxytosis/ferroptosis in AD, and potentially other diseases, because there simply have not been good gene sets available. In fact, this was one of the major reasons that led us to conduct our study. Oxytosis/ferroptosis has been poorly defined at the RNA level; therefore, the datasets are limited. Overlap of the FerrDb, TrioSig, and Ferroptosis signatures showed that they are quite distinct in composition. Importantly, while the FerrDb data set has been assembled through manual curation of the literature, the TrioSig genes were selected from a tri-culture brain cell model where oxytosis/ferroptosis was induced. Therefore, the expression of the genes in TrioSig is directly mechanistically related to this cell death pathway, which may help explain some of our key observations.

The TrioSig and FerrDb signatures were found enriched in specific AD brain regions, namely in the TCX, IFG, PHG, STG, and HP, but not in the other regions. This could reflect pathological alterations taking place in these regions that are related to oxytosis/ferroptosis as well as the time course of disease progression through the brain. It is interesting to note that the IFG is physically associated with the STG, and that the PHG surrounds the HP, one of the first regions in the brain to be affected in AD.

We saw that the TrioSig genes are highly expressed in several cell types (astrocytes, endothelial cells, microglia, neurons, and oligodendrocytes) under physiological conditions, but more so in microglia. Interestingly, the Hammond lab reported that microglia are particularly susceptible to oxytosis/ferroptosis [51]. However, our enrichment analysis with transcriptomic data from single-cell types in AD brain regions detected both the FerrDb and TrioSig signatures enriched in all of the different cell types investigated. This observation does not invalidate the idea that cell types contribute unevenly to AD pathology. Furthermore, the occurrence of oxytosis/ferroptosis-related stress in specific cell types could trigger unique responses. One of the two snRNA studies reported changes in the DNA damage response in excitatory neurons and oligodendrocytes as well as alterations in specific neuronal subpopulations in the AD prefrontal cortex [60]. The other study identified selectively vulnerable neurons in the AD entorhinal cortex associated with neurofibrillary inclusions during disease progression and discovered a subpopulation of reactive astrocytes [61]. Additional studies focused on single-cell transcriptomics in the prefrontal cortex of AD patients found changes related to angiogenesis, immune activation, myelination, and proteostasis across cell types [77–79]. Clearly, there is heterogeneity between these findings. This could be explained by variations in technical procedures, bioinformatic approaches, and number of nuclei sequenced.

Two recent studies have evaluated the enrichment of oxytotic/ferroptotic FerrDb genes in a small set of human AD whole brain transcriptomic data [80, 81]. Zhao et al. found the Ferroptosis and Apoptosis KEGG pathways enriched associated with genes upregulated in AD and identified several FerrDb genes as being DE [80]. Sun et al. overlapped DE genes in AD with the FerrDb gene set to identify hub genes that were also upregulated in AD and are involved in glutathione metabolism, cell cycle, cell differentiation, and immune activation [81]. These studies were not as thorough as ours and they did not include the TrioSig. Nonetheless, the relationship between oxytosis/ferroptosis and inflammation, which we did not explore because it was out of the scope of the current study, is of great interest and has been recently reviewed [82]. Activation of inflammatory signaling pathways, such as JAK-STAT, NF-κB, inflammasome, cGAS-STING, and MAPK signaling pathways, can lead to oxytosis/ferroptosis.

While cultured cells die rapidly following the induction of oxytosis/ferroptosis, it is possible that with aging and in AD patients oxytosis/ferroptosis takes place over an extended time period thereby leading to a slow degeneration of basic neuronal functions prior to cell death [4]. Although still poorly understood, the occurrence of oxytosis/ferroptosis-related stress at a chronic level with aging may be key to its contribution to disease. As such, future studies should use a similar approach to the one described here to address the enrichment of the Ferroptosis, FerrDb, and TrioSig signatures in various aging models.

Functional analysis of the TrioSig identified activation of the ISR in AD, which was confirmed in cell culture experiments. The ISR can be activated in response to a range of physiological changes and pathological conditions [62]. Phosphorylation of eIF2α is central to the ISR and can take place by one of the four eIF2α kinases: general control nonderepressible protein 2 (GCN2), double-stranded RNA-dependent protein kinase (PKR), PKR-like ER kinase (PERK), and heme-regulated eIF2α kinase (HRI). Although we did not investigate which of these kinases was behind the effects of glutamate, erastin, and RSL3 in HT22 cells, all of them can become activated due to oxidative stress in addition to responding to distinct environmental and physiological stresses [62]. ATF4 is the best characterized effector of the ISR and has a role in regulating metabolic and redox processes during the ISR [62]. Clearly, the fact that activation of the ISR involves increased expression of transcription factors such as ATF4 explains why it was picked up by our analyses, which was focused on transcriptomics. The outcome of ISR activation depends not only on the nature of the stress, its duration, and severity, but also on the extent of eIF2a phosphorylation, the translation of ATF4 mRNA or other transcription factors, and the translation and expression of their downstream targets. While a short activation of ISR is adaptive, a prolonged one can trigger cell death [62]. This could explain our observations that the apoptosis KEGG pathway was significantly enriched along with FerrDb and TrioSig in some of the models, including HT22 cells, MC65 cells, 5xFAD mice, and human AD brain tissues. Interestingly, when analyzing the snRNA data from mice and human AD brain tissues, apoptosis was no longer observed. Although the interaction between the ISR and cell death/pro-survival pathways has been somewhat studied [62], the crosstalk of these with oxytosis/ferroptosis requires further investigation.

Our observation that ISR activation may be part of a protective response in HT22 cells exposed to oxytosis/ferroptosis is in accordance with published data showing that fibroblasts expressing a nonphosphorylatable eIF2α have enhanced sensitivity to toxic insults such as glutamate and Aβ [83]. This correlated with impaired GSH synthesis and was demonstrated to require ATF4 [83, 84]. Increased activity of peIF2α/ATF4 was also shown to contribute to resistance of PC12 cells against Aβ. In MC65 cells, where intracellular aggregation of Aβ

induces oxytosis/ferroptosis, we also saw enrichment of the TrioSig and increased expression of ATF4. Importantly, pIF2α and ATF4 levels were found to be correlated and upregulated in human AD brains [83]. Evidence has demonstrated a significant role for ISR signaling as a hub involved in brain and behavioral impairments in AD [85], and it has been shown that the most prevalent genetic risk factor for AD, the ApoE4 allele, correlated with increased phosphorylation of eIF2α and increased mRNA expression of ATF4 [86]. In addition, the ISR also has a role in innate immunity to harness immune cells to produce inflammatory cytokines in response to microbial cues [87]. Interestingly, some inhibitors of oxytosis/ferroptosis seem to be protective by activating the ISR via peIF2α/ATF4 [83, 88]. Therefore, whether the ISR is an adaptive response against disease-related cellular stress or a cause of neurodegeneration still remains unclear. It likely depends on the context as well as the other players involved. It should be added that, as there are multiple ways of inducing the ISR, activation of the ISR in AD is not strictly indicative of activation of oxytosis/ferroptosis-related processes. The potential for these processes to operate in specific AD brain regions, as suggested by analysis of the TrioSig signature, requires further studies as more data from single-cell transcriptomics becomes available.

NRF2 is a key regulator of protective responses against oxidative stress that has been shown to inhibit oxytosis/ferroptosis in various cancer cell lines [66, 67]. Therefore, our observation that absence of NRF2 in HT22 cells increased the survival of HT22 cells exposed to oxytosis/ferroptosis was unexpected. We showed that in HT22 cells this was due to activation of HO1, a downstream effector of NRF2 that has also been shown to potentiate oxytosis/ferroptosis [68, 69]. On the other hand, removing NRF2 in MC65 cells enhanced Aβ toxicity, suggesting a protective role for NRF2 in these cells. Also unlike in HT22 cells, removing ATF4 in MC65 cells prevented some of the cell death. These differences in modulating the ISR in HT22 cells and MC65 cells could be explained by the duration of the ongoing ISR (a few hours in HT22 cells versus a few days in MC65 cells), which can have different outcomes as discussed above [62]. Clearly, further studies are required to understand the interplay between NRF2 and ATF4 during activation of the ISR in these models.

One potential caveat of the TrioSig is the fact that it was generated specifically from neurons, astrocytes, and microglia. Although the ISR has been observed ubiquitously, the use of the TrioSig signature to study transcriptomic data from other brain cell types or tissues other than the nervous system in future studies may be limited. As such, it would be important to compare the transcriptomic changes of varied cell types exposed to oxytosis/ferroptosis.

Conclusions

In conclusion, our data show an enrichment of transcriptomic signatures of oxytosis/ferroptosis in the brains of human AD patients, supporting the involvement of oxytosis/ferroptosis in the disease. These findings should be complemented with future studies with additional data from human brains as they become available as well as other types of omics data that also address the interaction of oxytosis/ferroptosis with aging. This is particularly relevant as there are strong concerns over the translational application of cell culture and animal systems to human AD. Importantly, we identified activation of the ISR as a mechanism triggered by oxytosis/ferroptosis that has also been observed in human AD studies. Therefore, the therapeutic potential of targeting the ISR to treat AD warrants further investigation.

Methods

Cell culture

HT22 mouse hippocampal nerve cells were cultured in high-glucose Dulbecco's modified Eagle's medium (DMEM) (Invitrogen, Carlsbad, CA, USA) supplemented with 10% fetal calf serum (FCS) (Hyclone, Logan, UT, USA) and incubated at 37°C in an atmosphere with 10% CO_2.

Oxytosis/ferroptosis

5×10^3 HT22 cells were plated per well in 96 well plates. After 24 h of culture, the medium was exchanged with fresh medium, and 5 mM glutamate, 500 nM erastin, or 250 nM RSL3 were added, as previously described [89]. Twenty-four hours later, the cellular viability was measured by the 3-(4,5-dimethylthiazolyl-2)-2,5-diphenyltetrazolium bromide (MTT) assay and confirmed microscopically.

Expression knock-down

HT22 cells were seeded in 60-mm dishes at a density of 5×10^5 cells/ml. Twenty-four hours after seeding, cells were transfected with siRNA against Atf4 (Santa Cruz, sc-351113, 17 pmol) or Nrf2 (Santa Cruz, sc-37049, 17 pmol), using lipofectamine (RNAiMAX, ThermoFisher) as the transfection reagent and Opti-MEM (GibcoTM) as the transfection medium. Control siRNA (Qiagen, 1027280) was used as a negative control. Cells were harvested 24 h after transfection and seeded into appropriate dishes for further study.

SDS-PAGE and immunoblotting

For western blotting, 3×10^5 HT22 cells per 60-mm dish were grown for 24 h prior to the indicated treatments. For nuclear extracts, cells were rinsed twice in ice-cold Tris-buffered saline (TBS), scraped into ice-cold nuclear fractionation buffer (10 mM HEPES, pH 7.9, 10 mM KCl, 0.1 mM EDTA, 0.1 mM EGTA, 1 mM DTT, 1 mM Na_3VO_4, 1 × protease inhibitor cocktail, and 1 × phosphatase inhibitor cocktail), and incubated on ice for 15 min. Then, NP40 at a final concentration of 0.6% was added, cells were vortexed, and the nuclei pelleted by centrifugation. Nuclear proteins were extracted by sonication of the nuclear pellet in nuclear fractionation buffer and the extracts were cleared by additional centrifugation. Total protein extracts were prepared by rinsing the cells twice with ice-cold phosphate-buffered saline. The cells were scraped into lysis buffer (50 mM HEPES, pH 7.5, 50 mM NaCl, 50 mM NaF, 10 mM Na pyrophosphate, 5 mM EDTA, 1% Triton X-100, 1 mM Na_3VO_4, 1 × protease inhibitor cocktail, 1 × phosphatase inhibitor cocktail) and incubated on ice for 30 min. Extracts were sonicated and cleared by centrifugation. The supernatants were stored at − 70°C until analysis. Protein concentrations were quantified by the bicinchoninic acid method (Pierce) and adjusted to equal concentrations. 5 × western blot sample buffer (74 mM Tris–HCl, pH 8.0, 6.25% SDS, 10% β-mercaptoethanol, 20% glycerol) was added to a final concentration of 2.5 × and samples were boiled for 5 min. Western blots were performed as previously described [90]. The primary antibodies used were β-actin HRP conjugate (1/20,000, Cell Signaling #5125), eIF2a (1/1000, Cell Signaling #2103), phospho-eIF2a (1/1000, Cell Signaling #9721), ATF4 (1/500, Santa Cruz #sc-200), and NRF2 (1/1000, Santa Cruz #13,032). Horseradish peroxidase-conjugated secondary goat anti-rabbit and goat anti-mouse (1:5000, Bio-Rad, 1,706,516, 1,721,019) antibodies were used.

Whole transcriptome analysis

Data with HT22 cells were generated as following. The original sources for all other data used are cited in the text. RNA was isolated from HT22 nerve cells using the RNeasy Plus Universal mini kit (Qiagen). RNA-Seq libraries were prepared using the Illumina TruSeq Stranded mRNA Sample Prep Kit according to the manufacturer's instructions. Briefly, poly-A RNA was selected using poly dT-beads. mRNA was then fragmented and reverse transcribed. cDNA was end-repaired, adenylated, and ligated with Illumina adapters with indexes. Adapter-ligated cDNA was then amplified. Libraries were pooled and sequenced single-end 50 base-pair (bp) on the Illumina HiSeq 2500 platform.

RNA-Seq reads were mapped by STAR [v2.5.3a, ref: https://doi.org/10.1093/bioinformatics/bts635. pmid:23104886] to the mm10 reference genome with default parameters and flag "–outFilterIntronMotifs RemoveNoncanonical." Homer [v4.9.1, ref: PMID: 20,513,432; http://homer.ucsd.edu/homer/] commands "makeTagDirectory" and "analyzeRepeats" were used to quantify gene expression by counting uniquely mapped reads across all exons of RefSeq genes. Differential expression analysis was performed using DESeq2 [v1.21.22, https://genomebiology.biomedcentral.com/articles/10.1186/s13059-014-0550-8.]. Genes with log fold change (logFC) > 0.5 and false discovery rate (FDR) < 0.05 were identified as significantly changed.

Bioinformatics and statistics

Over-representation analysis (ORA) was performed using WebGestalt (https://www.webgestalt.org). To determine the enrichment of the TrioSig and FerrDb signatures, a functional database including these two signatures and all the KEGG pathways was used. Pathways with FDR < 0.05 were identified as significantly changed. In the text figures, only the significance for FerrDb, TrioSig, Ferroptosis, Apoptosis, Necroptosis, and Autophagy is shown. Gene ontology analysis was performed using WebGestalt. For ingenuity pathway analysis (IPA), the TrioSig dataset genes with respective direction of expression were imported into IPA (Qiagen, Redwood City, CA, USA) and analyzed for a comprehensive look at enriched pathways. Where appropriate, experiments were performed at least three independent times. GraphPad Prism 10 was used for statistical analysis and exact *P* values are indicated (for $P < 0.050$).

Supplementary Information

The online version contains supplementary material available at https://doi.org/10.1186/s12915-025-02235-6.

Additional file 1: Fig. S1 Overlap of the gene sets from TrioSig, FerrDb, and Ferroptosis with the gene sets from Apoptosis, Autophagy, and Necroptosis to identify the number of genes shared

Additional file 2: Fig. S2 Transcriptomic enrichment of TrioSig Down and TrioSig Up in the (A) cell culture models, (B) AD mouse models, (C) human AD brain regions, (D) brain cell types of 5xFAD mice, and (E) brain cell types of human AD brain regions. HP, hippocampus; RS CX, retrosplenial cortex; ICX, insular cortex; HB, hemibrain; CBE, cerebellum; TCX, temporal cortex; DLPFC, dorsolateral prefrontal cortex; ACC, anterior cingulate cortex; PCC, posterior cingulate cortex; FP, frontal pole; IFG, inferior frontal gyrus; PHG, parahippocampal gyrus; STG, superior temporal gyrus; HP, hippocampus; DG, dentate gyrus; CA, cornu ammonis; PFC, prefrontal cortex; SFG, superior frontal gyrus; EC, caudal entorhinal cortex

Additional file 3: Fig. S3 Visualization of the TrioSig signature in the eIF2 signaling pathway

Additional file 4: Fig. S4 Visualization of the TrioSig signature in the NFE2L2 regulating antioxidant/detoxification enzymes pathway

Additional file 5: Fig. S5 The role of HO1 in oxytosis/ferroptosis in HT22 cells. (A) Levels of HO1 and actin after treatment of HT22 cells with 5 mM and 7.5 mM glutamate, 250 nM erastin, and 500 nM and 750 nM RSL3 assessed by western blotting and quantified after knockdown with control (Ct) or Nrf2 siRNAs ($n = 3$/condition). (B) Survival of HT22 cells exposed to 7.5 mM glutamate, 500 nM erastin, or 250 nM RSL3 in the absence and presence of 10 μM ZnPPIX ($n = 3$/condition). (C) Survival of HT22 cells exposed to varying concentrations of glutamate, erastin, or RSL3 after knockdown with Ct or HO1 siRNAs ($n = 3$/condition). Two-way repeated measures ANOVA and Tukey's multiple comparisons test, $^{*}P < 0.05$, $^{**}P < 0.01$, $^{***}P < 0.001$, $^{****}P < 0.0001$. All data are mean ± SD

Additional file 6: Table S1 List of the mouse and human gene sets for the TrioSig, TrioSig Down, TrioSig Up, FerrDb, Ferroptosis, Apoptosis, Autophagy, and Necroptosis signatures

Additional file 7: Table S2 List of all genes DE between HT22 mouse hippocampal nerve cells non-induced and induced to undergo oxytosis/ferroptosis (with glutamate 5 mM). log2FC, logarithm to base 2 of fold change; p_val_adj, adjusted *P* value

Additional file 8: Table S3 List of all genes DE between MC65 human neuroblastoma cells non-induced and induced to aggregate Aβ intracellularly. log2FC, logarithm to base 2 of fold change; *p*_val_adj, adjusted *P* value

Additional file 9: Western blots

Acknowledgements
We thank Dr. Timothy Hammond for providing data on the DE genes from human microglia, astrocytes and neurons. This work was supported by the Bundy Foundation (D.S.) and grants from the NIH (AG067331 for A.C., AG069206 and AG061296 for P.M.). The results published here are in part based on data obtained from the AD Knowledge Portal (https://doi.org/https://doi.org/10.7303/syn2580853).

Authors' contributions
AC conceived the project, performed data analysis, interpretation of data and wrote the manuscript. KS performed pathway analysis. DSC performed data analysis. NJD performed data analysis. KGE performed RNAseq alignment and statistical analysis. SS performed pathway analysis and interpretation of data. All authors read, edited and approved the manuscript. PM conceived the project, performed experiments and interpretation of data.

Funding
This work was supported by the Bundy Foundation (DS) and grants from the NIH (AG067331 for AC, R25GM060507 for KS, AG069206 and AG061296 for PM).

Data Availability
RNA-Seq raw data from HT22 cells was deposited at Gene Expression Omnibus (GEO) with accession number GSE278716.

Declarations

Competing interests
The authors declare no competing interests.

Received: 4 December 2024 Accepted: 6 May 2025
Published online: 14 May 2025

References

1. Tan S, Sagara Y, Liu Y, Maher P, Schubert D. The regulation of reactive oxygen species production during programmed cell death. J Cell Biol. 1998;141(6):1423–32.
2. Tan S, Schubert D, Maher P. Oxytosis: a novel form of programmed cell death. Curr Top Med Chem. 2001;1(6):497–506.
3. Lewerenz J, Ates G, Methner A, Conrad M, Maher P. Oxytosis/ferroptosis-(re-) emerging roles for oxidative stress-dependent non-apoptotic cell death in diseases of the central nervous system. Front Neurosci. 2018;12:214.
4. Maher P, Currais A, Schubert D. Using the oxytosis/ferroptosis pathway to understand and treat age-associated neurodegenerative diseases. Cell Chem Biol. 2020;27(12):1456–71.
5. Dixon SJ, Lemberg KM, Lamprecht MR, Skouta R, Zaitsev EM, Gleason CE, Patel DN, Bauer AJ, Cantley AM, Yang WS, et al. Ferroptosis: an iron-dependent form of nonapoptotic cell death. Cell. 2012;149(5):1060–72.
6. Yang WS, SriRamaratnam R, Welsch ME, Shimada K, Skouta R, Viswanathan VS, Cheah JH, Clemons PA, Shamji AF, Clish CB, et al. Regulation of ferroptotic cancer cell death by GPX4. Cell. 2014;156(1–2):317–31.
7. Pedrera L, Ros U, Garcia-Saez AJ. Calcium as a master regulator of ferroptosis and other types of regulated necrosis. Cell Calcium. 2023;114:102778.
8. Ashraf A, Jeandriens J, Parkes HG, So PW. Iron dyshomeostasis, lipid peroxidation and perturbed expression of cystine/glutamate antiporter in Alzheimer's disease: evidence of ferroptosis. Redox Biol. 2020;32:101494.
9. Chen K, Jiang X, Wu M, Cao X, Bao W, Zhu LQ. Ferroptosis, a potential therapeutic target in Alzheimer's disease. Front Cell Dev Biol. 2021;9:704298.
10. Conrad M, Lorenz SM, Proneth B. Targeting ferroptosis: new hope for as-yet-incurable diseases. Trends Mol Med. 2021;27(2):113–22.
11. Majernikova N, den Dunnen WFA, Dolga AM. The potential of ferroptosis-targeting therapies for Alzheimer's disease: from mechanism to transcriptomic analysis. Front Aging Neurosci. 2021;13:745046.
12. Zhang G, Zhang Y, Shen Y, Wang Y, Zhao M, Sun L. The potential role of ferroptosis in Alzheimer's disease. J Alzheimers Dis. 2021;80(3):907–25.
13. Ballatori N, Krance SM, Notenboom S, Shi S, Tieu K, Hammond CL. Glutathione dysregulation and the etiology and progression of human diseases. Biol Chem. 2009;390(3):191–214.
14. Ansari MA, Scheff SW. Oxidative stress in the progression of Alzheimer disease in the frontal cortex. J Neuropathol Exp Neurol. 2010;69(2):155–67.
15. Emir UE, Raatz S, McPherson S, Hodges JS, Torkelson C, Tawfik P, White T, Terpstra M. Noninvasive quantification of ascorbate and glutathione concentration in the elderly human brain. NMR Biomed. 2011;24(7):888–94.
16. Currais A, Maher P. Functional consequences of age-dependent changes in glutathione status in the brain. Antioxid Redox Signal. 2013;19(8):813–22.
17. Mandal PK, Saharan S, Tripathi M, Murari G. Brain glutathione levels–a novel biomarker for mild cognitive impairment and Alzheimer's disease. Biol Psychiatry. 2015;78(10):702–10.
18. Maher P. The effects of stress and aging on glutathione metabolism. Ageing Res Rev. 2005;4(2):288–314.
19. Droge W, Kinscherf R, Hildebrandt W, Schmitt T. The deficit in low molecular weight thiols as a target for antiageing therapy. Curr Drug Targets. 2006;7(11):1505–12.
20. Giustarini D, Dalle-Donne I, Lorenzini S, Milzani A, Rossi R. Age-related influence on thiol, disulfide, and protein-mixed disulfide levels in human plasma. J Gerontol A Biol Sci Med Sci. 2006;61(10):1030–8.
21. Sekhar RV, Patel SG, Guthikonda AP, Reid M, Balasubramanyam A, Taffet GE, Jahoor F. Deficient synthesis of glutathione underlies oxidative stress in aging and can be corrected by dietary cysteine and glycine supplementation. Am J Clin Nutr. 2011;94(3):847–53.
22. Bermejo P, Martin-Aragon S, Benedi J, Susin C, Felici E, Gil P, Ribera JM, Villar AM. Peripheral levels of glutathione and protein oxidation as markers in the development of Alzheimer's disease from mild cognitive impairment. Free Radic Res. 2008;42(2):162–70.
23. Rae CD, Williams SR. Glutathione in the human brain: review of its roles and measurement by magnetic resonance spectroscopy. Anal Biochem. 2017;529:127–43.
24. Bradley MA, Markesbery WR, Lovell MA. Increased levels of 4-hydroxynonenal and acrolein in the brain in preclinical Alzheimer disease. Free Radic Biol Med. 2010;48(12):1570–6.
25. Sultana R, Perluigi M, Butterfield DA. Lipid peroxidation triggers neurodegeneration: a redox proteomics view into the Alzheimer disease brain. Free Radic Biol Med. 2013;62:157–69.
26. Bradley-Whitman MA, Lovell MA. Biomarkers of lipid peroxidation in Alzheimer disease (AD): an update. Arch Toxicol. 2015;89(7):1035–44.
27. Gaschler MM, Stockwell BR. Lipid peroxidation in cell death. Biochem Biophys Res Commun. 2017;482(3):419–25.

28. Joshi YB, Pratico D. The 5-lipoxygenase pathway: oxidative and inflammatory contributions to the Alzheimer's disease phenotype. Front Cell Neurosci. 2014;8:436.
29. Joshi YB, Giannopoulos PF, Pratico D. The 12/15-lipoxygenase as an emerging therapeutic target for Alzheimer's disease. Trends Pharmacol Sci. 2015;36(3):181–6.
30. Kuhn H, Banthiya S, van Leyen K. Mammalian lipoxygenases and their biological relevance. Biochim Biophys Acta. 2015;1851(4):308–30.
31. Singh NK, Rao GN. Emerging role of 12/15-lipoxygenase (ALOX15) in human pathologies. Prog Lipid Res. 2019;73:28–45.
32. Liang Z, Soriano-Castell D, Kepchia D, Duggan BM, Currais A, Schubert D, Maher P. Cannabinol inhibits oxytosis/ferroptosis by directly targeting mitochondria independently of cannabinoid receptors. Free Radic Biol Med. 2022;180:33–51.
33. Costantini LC, Barr LJ, Vogel JL, Henderson ST. Hypometabolism as a therapeutic target in Alzheimer's disease. BMC Neurosci. 2008;9(Suppl 2):S16.
34. Cunnane S, Nugent S, Roy M, Courchesne-Loyer A, Croteau E, Tremblay S, Castellano A, Pifferi F, Bocti C, Paquet N, et al. Brain fuel metabolism, aging, and Alzheimer's disease. Nutrition. 2011;27(1):3–20.
35. Yin F, Boveris A, Cadenas E. Mitochondrial energy metabolism and redox signaling in brain aging and neurodegeneration. Antioxid Redox Signal. 2014;20(2):353–71.
36. Currais A. Ageing and inflammation - a central role for mitochondria in brain health and disease. Ageing Res Rev. 2015;21:30–42.
37. Hagemeier J, Geurts JJ, Zivadinov R. Brain iron accumulation in aging and neurodegenerative disorders. Expert Rev Neurother. 2012;12(12):1467–80.
38. Hare D, Ayton S, Bush A, Lei P. A delicate balance: iron metabolism and diseases of the brain. Front Aging Neurosci. 2013;5:34.
39. Gleason A, Bush AI. Iron and ferroptosis as therapeutic targets in Alzheimer's disease. Neurotherapeutics. 2021;18(1):252–64.
40. Good PF, Perl DP, Bierer LM, Schmeidler J. Selective accumulation of aluminum and iron in the neurofibrillary tangles of Alzheimer's disease: a laser microprobe (LAMMA) study. Ann Neurol. 1992;31(3):286–92.
41. Tao Y, Wang Y, Rogers JT, Wang F. Perturbed iron distribution in Alzheimer's disease serum, cerebrospinal fluid, and selected brain regions: a systematic review and meta-analysis. J Alzheimers Dis. 2014;42(2):679–90.
42. Raven EP, Lu PH, Tishler TA, Heydari P, Bartzokis G. Increased iron levels and decreased tissue integrity in hippocampus of Alzheimer's disease detected in vivo with magnetic resonance imaging. J Alzheimers Dis. 2013;37(1):127–36.
43. Ayton S, Wang Y, Diouf I, Schneider JA, Brockman J, Morris MC, Bush AI. Brain iron is associated with accelerated cognitive decline in people with Alzheimer pathology. Mol Psychiatry. 2020;25(11):2932–41.
44. Huang L, McClatchy DB, Maher P, Liang Z, Diedrich JK, Soriano-Castell D, Goldberg J, Shokhirev M, Yates JR 3rd, Schubert D, et al. Intracellular amyloid toxicity induces oxytosis/ferroptosis regulated cell death. Cell Death Dis. 2020;11(10):828.
45. Seiler A, Schneider M, Forster H, Roth S, Wirth EK, Culmsee C, Plesnila N, Kremmer E, Radmark O, Wurst W, et al. Glutathione peroxidase 4 senses and translates oxidative stress into 12/15-lipoxygenase dependent- and AIF-mediated cell death. Cell Metab. 2008;8(3):237–48.
46. Hambright WS, Fonseca RS, Chen L, Na R, Ran Q. Ablation of ferroptosis regulator glutathione peroxidase 4 in forebrain neurons promotes cognitive impairment and neurodegeneration. Redox Biol. 2017;12:8–17.
47. Maher P. Inhibitors of oxytosis/ferroptosis: a new class of therapeutics for Alzheimer's disease. In: Tang D, editor. Ferroptosis in Health and Disease. Cham: Springer International Publishing; 2023. p. 461–90.
48. Currais A, Raschke W, Maher P. CMS121, a novel drug candidate for the treatment of Alzheimer's disease and age-related dementia. J Alzheimers Dis. 2024;101(s1):S179–92.
49. Zhou N, Bao J. FerrDb: a manually curated resource for regulators and markers of ferroptosis and ferroptosis-disease associations. Database (Oxford). 2020;2020:baaa021.
50. Zhou N, Yuan X, Du Q, Zhang Z, Shi X, Bao J, Ning Y, Peng L. FerrDb V2: update of the manually curated database of ferroptosis regulators and ferroptosis-disease associations. Nucleic Acids Res. 2023;51(D1):D571–82.
51. Ryan SK, Zelic M, Han Y, Teeple E, Chen L, Sadeghi M, Shankara S, Guo L, Li C, Pontarelli F, et al. Microglia ferroptosis is regulated by SEC24B and contributes to neurodegeneration. Nat Neurosci. 2023;26(1):12–26.
52. Lee S, Hwang N, Seok BG, Lee S, Lee SJ, Chung SW. Autophagy mediates an amplification loop during ferroptosis. Cell Death Dis. 2023;14(7):464.
53. McKenzie AT, Wang M, Hauberg ME, Fullard JF, Kozlenkov A, Keenan A, Hurd YL, Dracheva S, Casaccia P, Roussos P, et al. Brain cell type specific gene expression and co-expression network architectures. Sci Rep. 2018;8(1):8868.
54. MODEL-AD consortium, https://sagebio.shinyapps.io/MODEL_AD_Explorer/#.
55. Papazoglou A, Henseler C, Weickhardt S, Teipelke J, Papazoglou P, Daubner J, Schiffer T, Krings D, Broich K, Hescheler J, et al. Sex- and region-specific cortical and hippocampal whole genome transcriptome profiles from control and APP/PS1 Alzheimer's disease mice. PLoS ONE. 2024;19(2):e0296959.
56. Yin W, Cerda-Hernandez N, Castillo-Morales A, Ruiz-Tejada-Segura ML, Monzon-Sandoval J, Moreno-Castilla P, Perez-Ortega R, Bermudez-Rattoni F, Urrutia AO, Gutierrez H. Transcriptional, behavioral and biochemical profiling in the 3xTg-AD mouse model reveals a specific signature of amyloid deposition and functional decline in Alzheimer's disease. Front Neurosci. 2020;14:602642.
57. van Rooij JGJ, Meeter LHH, Melhem S, Nijholt DAT, Wong TH, Netherlands Brain B, Rozemuller A, Uitterlinden AG, van Meurs JG, van Swieten JC. Hippocampal transcriptome profiling combined with protein-protein interaction analysis elucidates Alzheimer's disease pathways and genes. Neurobiol Aging. 2019;74:225–33.
58. Agora, https://agora.adknowledgeportal.org.
59. Zhou Y, Song WM, Andhey PS, Swain A, Levy T, Miller KR, Poliani PL, Cominelli M, Grover S, Gilfillan S, et al. Human and mouse single-nucleus transcriptomics reveal TREM2-dependent and TREM2-independent cellular responses in Alzheimer's disease. Nat Med. 2020;26(1):131–42.
60. Mathys H, Peng Z, Boix CA, Victor MB, Leary N, Babu S, Abdelhady G, Jiang X, Ng AP, Ghafari K, et al. Single-cell atlas reveals correlates of high cognitive function, dementia, and resilience to Alzheimer's disease pathology. Cell. 2023;186(20):4365-4385 e4327.
61. Leng K, Li E, Eser R, Piergies A, Sit R, Tan M, Neff N, Li SH, Rodriguez RD, Suemoto CK, et al. Molecular characterization of selectively vulnerable neurons in Alzheimer's disease. Nat Neurosci. 2021;24(2):276–87.
62. Pakos-Zebrucka K, Koryga I, Mnich K, Ljujic M, Samali A, Gorman AM. The integrated stress response. EMBO Rep. 2016;17(10):1374–95.
63. Kress JKC, Jessen C, Hufnagel A, Schmitz W, Xavier da Silva TN, Ferreira Dos Santos A, Mosteo L, Goding CR, Friedmann Angeli JP, Meierjohann S: The integrated stress response effector ATF4 is an obligatory metabolic activator of NRF2. Cell Rep. 2023;42(7):112724.
64. Liu J, Song X, Kuang F, Zhang Q, Xie Y, Kang R, Kroemer G, Tang D. NUPR1 is a critical repressor of ferroptosis. Nat Commun. 2021;12(1):647.
65. Ehren JL, Maher P. Concurrent regulation of the transcription factors Nrf2 and ATF4 mediates the enhancement of glutathione levels by the flavonoid fisetin. Biochem Pharmacol. 2013;85(12):1816–26.
66. Anandhan A, Dodson M, Shakya A, Chen J, Liu P, Wei Y, Tan H, Wang Q, Jiang Z, Yang K, et al. NRF2 controls iron homeostasis and ferroptosis through HERC2 and VAMP8. Sci Adv. 2023;9(5):eade9585.
67. Dodson M, Castro-Portuguez R, Zhang DD. NRF2 plays a critical role in mitigating lipid peroxidation and ferroptosis. Redox Biol. 2019;23:101107.
68. Kwon MY, Park E, Lee SJ, Chung SW. Heme oxygenase-1 accelerates erastin-induced ferroptotic cell death. Oncotarget. 2015;6(27):24393–403.
69. Wu D, Hu Q, Wang Y, Jin M, Tao Z, Wan J. Identification of HMOX1 as a critical ferroptosis-related gene in atherosclerosis. Front Cardiovasc Med. 2022;9:833642.
70. Wan YW, Al-Ouran R, Mangleburg CG, Perumal TM, Lee TV, Allison K, Swarup V, Funk CC, Gaiteri C, Allen M, et al. Meta-analysis of the Alzheimer's disease human brain transcriptome and functional dissection in mouse models. Cell Rep. 2020;32(2):107908.
71. Conway OJ, Carrasquillo MM, Wang X, Bredenberg JM, Reddy JS, Strickland SL, Younkin CS, Burgess JD, Allen M, Lincoln SJ, et al. ABI3 and PLCG2 missense variants as risk factors for neurodegenerative diseases in Caucasians and African Americans. Mol Neurodegener. 2018;13(1):53.
72. Patrick E, Olah M, Taga M, Klein HU, Xu J, White CC, Felsky D, Agrawal S, Gaiteri C, Chibnik LB, et al. A cortical immune network map identifies distinct microglial transcriptional programs associated with beta-amyloid and tau pathologies. Transl Psychiatry. 2021;11(1):50.
73. Milind N, Preuss C, Haber A, Ananda G, Mukherjee S, John C, Shapley S, Logsdon BA, Crane PK, Carter GW. Transcriptomic stratification of

late-onset Alzheimer's cases reveals novel genetic modifiers of disease pathology. PLoS Genet. 2020;16(6):e1008775.
74. Sekar S, McDonald J, Cuyugan L, Aldrich J, Kurdoglu A, Adkins J, Serrano G, Beach TG, Craig DW, Valla J, et al. Alzheimer's disease is associated with altered expression of genes involved in immune response and mitochondrial processes in astrocytes. Neurobiol Aging. 2015;36(2):583–91.
75. Scheltens P, De Strooper B, Kivipelto M, Holstege H, Chetelat G, Teunissen CE, Cummings J, van der Flier WM. Alzheimer's disease. Lancet. 2021;397(10284):1577–90.
76. Kinney JW, Bemiller SM, Murtishaw AS, Leisgang AM, Salazar AM, Lamb BT. Inflammation as a central mechanism in Alzheimer's disease. Alzheimers Dement (N Y). 2018;4:575–90.
77. Mathys H, Davila-Velderrain J, Peng Z, Gao F, Mohammadi S, Young JZ, Menon M, He L, Abdurrob F, Jiang X, et al. Single-cell transcriptomic analysis of Alzheimer's disease. Nature. 2019;570(7761):332–7.
78. Lau SF, Cao H, Fu AKY, Ip NY. Single-nucleus transcriptome analysis reveals dysregulation of angiogenic endothelial cells and neuroprotective glia in Alzheimer's disease. Proc Natl Acad Sci U S A. 2020;117(41):25800–9.
79. Sziraki A, Lu Z, Lee J, Banyai G, Anderson S, Abdulraouf A, Metzner E, Liao A, Banfelder J, Epstein A, et al. A global view of aging and Alzheimer's pathogenesis-associated cell population dynamics and molecular signatures in human and mouse brains. Nat Genet. 2023;55(12):2104–16.
80. Zhao H, Wang J, Li Z, Wang S, Yu G, Wang L. Identification ferroptosis-related hub genes and diagnostic model in Alzheimer's disease. Front Mol Neurosci. 2023;16:1280639.
81. Sun Y, Xiao Y, Tang Q, Chen W, Lin L. Genetic markers associated with ferroptosis in Alzheimer's disease. Front Aging Neurosci. 2024;16:1364605.
82. Chen Y, Fang ZM, Yi X, Wei X, Jiang DS. The interaction between ferroptosis and inflammatory signaling pathways. Cell Death Dis. 2023;14(3):205.
83. Lewerenz J, Maher P. Basal levels of eIF2alpha phosphorylation determine cellular antioxidant status by regulating ATF4 and xCT expression. J Biol Chem. 2009;284(2):1106–15.
84. Lewerenz J, Sato H, Albrecht P, Henke N, Noack R, Methner A, Maher P. Mutation of ATF4 mediates resistance of neuronal cell lines against oxidative stress by inducing xCT expression. Cell Death Differ. 2012;19(5):847–58.
85. Lourenco MV, Ferreira ST, De Felice FG. Neuronal stress signaling and eIF2alpha phosphorylation as molecular links between Alzheimer's disease and diabetes. Prog Neurobiol. 2015;129:37–57.
86. Segev Y, Barrera I, Ounallah-Saad H, Wibrand K, Sporild I, Livne A, Rosenberg T, David O, Mints M, Bramham CR, et al. PKR inhibition rescues memory deficit and ATF4 overexpression in ApoE epsilon4 human replacement mice. J Neurosci. 2015;35(38):12986–93.
87. Abdel-Nour M, Carneiro LAM, Downey J, Tsalikis J, Outlioua A, Prescott D, Da Costa LS, Hovingh ES, Farahvash A, Gaudet RG, et al. The heme-regulated inhibitor is a cytosolic sensor of protein misfolding that controls innate immune signaling. Science. 2019;365(6448):eaaw4144.
88. Valera E, Dargusch R, Maher PA, Schubert D. Modulation of 5-lipoxygenase in proteotoxicity and Alzheimer's disease. J Neurosci. 2013;33(25):10512–25.
89. Soriano-Castell D, Liang Z, Maher P, Currais A. Profiling the chemical nature of anti-oxytotic/ferroptotic compounds with phenotypic screening. Free Radic Biol Med. 2021;177:313–25.
90. Currais A, Huang L, Goldberg J, Petrascheck M, Ates G, Pinto-Duarte A, Shokhirev MN, Schubert D, Maher P. Elevating acetyl-CoA levels reduces aspects of brain aging. Elife. 2019;8:e47866.

Publisher's Note